DOI: 10.1002/ejic.200700108

Influence of the Synthetic Pathway on the Properties of Oxygen-Deficient Manganese-Related Perovskites

José M. Alonso,[a,b] Raquel Cortés-Gil,[a,c] Luisa Ruiz-González,[c] José M. González-Calbet,*,[a,c] Antonio Hernando,[a,d] María Vallet-Regí,[a,e] María E. Dávila,[b] and María C. Asensio[b,f]

Keywords: Mixed-valent compounds / Perovskite phases / Magnetic properties / X-ray absorption near-edge spectroscopy (XANES) / Topotactic reaction

Thermogravimetry, X-ray and electron diffraction and high resolution electron microscopy show that the reduction process from perovskite $La_{0.5}Ca_{0.5}MnO_3$ to brownmillerite $La_{0.5}Ca_{0.5}MnO_{2.5}$ is a reversible topotactic process. Two series of monophasic $La_{0.5}Ca_{0.5}MnO_{3-\delta}$ oxygen-deficient perovskites were stabilized in the $0 \leq \delta \leq 0.12$ range, either from reduction of $La_{0.5}Ca_{0.5}MnO_3$ or oxidation of $La_{0.5}Ca_{0.5}MnO_{2.5}$. Soft X-ray absorption spectroscopy shows that Mn oxidation states differ as a function of the synthetic pathway. Temperature dependence of the magnetization as a function of anionic vacancies concentration at constant doping level are reported together with the evolution of high-resolution O K-edge and Mn L-edge spectra. Our results show dramatic changes in the magnetic behaviour due to the stabilization of different Mn oxidation states.

Introduction

The influence of cationic substitution and anionic vacancies on the magnetic and conducting properties of transition-metal oxides is a subject of high scientific and technological interest. The main objective of most of these studies is to get a precise understanding of the nominal composition, microstructure and electronic properties of intriguing and complex materials, as in the case of manganese-related perovskites. These materials exhibit a wide range of unusual magnetic properties, which can be modified by changing the doping level due to the long-established ability of the manganese ion to develop several oxidation states. This essential property could be directly related to the number of unpaired electrons in the 3d orbitals, as well as to the magnetic moment associated with each of the Mn ions present in the compound.

Particularly interesting in the $La_{1-x}Ca_xMnO_3$ system is the $La_{0.5}Ca_{0.5}MnO_3$ material, which shows a remarkable coexistence of ferromagnetism and charge ordered (CO) phase.[1–4] At this state, the 1:1 arrangement of octahedrally coordinated Mn^{3+} and Mn^{4+} leads to charge and orbital order at low temperature. However, some authors disagree with this general description.[5–8]

From a magnetic point of view, CO represents the limit between ferromagnetic (FM) metallic (M) and antiferromagnetic (AF) insulator (I) behaviour.[9,10] The shift towards one behaviour or the other is obtained by varying the Mn^{4+}/Mn^{3+} ratio. Thus, when such a ratio verifies $0.20 < Mn^{4+}/Mn^{3+} < 1$, the system is FM-M, whereas values of $Mn^{4+}/Mn^{3+} \geq 1$ give rise to an AF-I system. To modify the concentration of doped holes (Mn^{4+} ions), it suffices to change the x value. However, introducing anionic vacancies can also modify this ratio. Actually, for a small concentration of anionic vacancies, the FM fraction in $La_{0.5}Ca_{0.5}MnO_{3-\delta}$ increases as the CO fraction decreases; this effect yields a net FM behaviour, related in turn to the decrease in the Mn^{4+}/Mn^{3+} ratio.[11,12] Despite experimental effort, a clear relationship between the CO state in $La_{0.5}Ca_{0.5}MnO_{3-\delta}$ and the valence d-configuration of the Mn ions is still missing.

In a previous paper,[13] it was shown that the reduction process of $La_{0.5}Ca_{0.5}Mn^{4+}{}_{0.5}Mn^{3+}{}_{0.5}O_{3-\delta}$ down to an oxy-

[a] Instituto de Magnetismo Aplicado (UCM-CSIC-ADIF), Las Rozas, P. O. Box 155, 28230 Madrid, Spain
Fax: +34-91-300-71-76
E-mail: josea@adif.es
[b] Instituto de Ciencia de Materiales (CSIC), 28049 Cantoblanco, Madrid, Spain
[c] Dpto. Química Inorgánica, Facultad de Químicas, Universidad Complutense, 28040 Madrid, Spain
Fax: +34-91-394-43-52
E-mail: jgcalbet@quim.ucm.es
[d] Dpto. Física de Materiales, Facultad de Físicas, Universidad Complutense, 28040 Madrid, Spain
[e] Dpto. Química Inorgánica y Bioinorgánica, Facultad de Farmacia, Universidad Complutense, 28040 Madrid, Spain
Fax: +34-91-394-17-86
E-mail: vallet@farm.ucm.es
[f] Synchroton SOLEIL, B. P. 48, 91192 Gif sur Yvette Cedex, France

gen deficiency $\delta = 0.5$ gave rise to a new oxide with the composition $La_{0.5}Ca_{0.5}MnO_{2.5}$, isostructural to $Sr_2Fe_2O_5$.[14] This reduction process is a topotactic one since the perovskite framework is kept as the oxygen content decreases, that is, the reduction pathway involves ordering of the anionic vacancies through the tetrahedra formation leading to the basic sequence ···OT··· (O = octahedron and T = tetrahedron) of the brownmillerite structure. Different topotactic processes have been already described for other Mn-related perovskite oxides. A well-known example is the case of $CaMnO_3$ which is transformed into $CaMnO_{2.5}$ through the formation of squared pyramids.[15] Another example is the reduction process of $LaMnO_3$ to $LaMnO_{2.75}$ which involves tetrahedra formation.[16] Moreover in $La_{0.5}Ca_{0.5}MnO_{2.5}$, Mn shows an average oxidation state of 2.5 which, according to the structural data,[13] could fit to contents of 75% of Mn^{2+} and 25% of Mn^{4+}. Taking this into account, the reduction process $La_{0.5}Ca_{0.5}Mn^{4+}_{0.5}Mn^{3+}_{0.5}O_3 \rightarrow La_{0.5}Ca_{0.5}Mn^{4+}_{0.25}Mn^{2+}_{0.75}O_{2.5}$ obviously involves the coexistence of Mn^{4+}, Mn^{3+} and Mn^{2+} for certain oxygen contents. Although rather unusual, the coexistence of a single metallic cation in three different oxidation states within a mixed oxide has been suggested by some authors in $Ln_{1-x}A_xMnO_3$ systems, as a consequence of the Mn^{3+} disproportion.[17] Moreover, such behaviour was previously observed in the oxygen-deficient perovskite $CaLaMgMnO_{6-\delta}$[18] and also in the solid solution goethite-groutite α-$Mn_xFe_{1-x}OOH$.[19] In order to confirm this assertion for $La_{0.5}Ca_{0.5}MnO_{2.5}$, which is basic to understanding the magnetic behaviour, further experimental evidence of the manganese oxidation state is clearly needed.

In this sense, it is well known that one of the most useful tools in the study of the atom-resolved unoccupied electronic structure of multi-element compounds is X-ray absorption fine structure spectroscopy. By tuning the photon energy to the threshold of a specific element, the shape of the absorption spectrum by its X-ray absorption near-edge spectroscopy (XANES) gives the electronic structure projected onto this particular site. This projection is usually strongly influenced by the hybridization between the states of different atoms, for complex multicomponent compounds. Because of the site- and symmetry-selective character of XANES, a simultaneous Mn L-edge and O K-edge study can give information about the manganese oxidation state and slight structural changes induced by cationic doping and anionic vacancies. This XANES ability has been previously illustrated by numerous studies on doped manganites.[20–23]

In this work, the Mn oxidation states and the magnetic properties of several $La_{0.5}Ca_{0.5}MnO_{3-\delta}$ materials as a function of the synthetic pathway were studied. In this sense, we prepared samples with the same oxygen content through two different methods: (i) reduction of $La_{0.5}Ca_{0.5}MnO_3$ and (ii) oxidation of $La_{0.5}Ca_{0.5}MnO_{2.5}$. The evolution of high-resolution O K-edge and Mn L-edge X-ray absorption spectroscopy as a function of anionic vacancies concentration at constant doping level is reported.

Results and Discussion

The powder XRD pattern corresponding to the $La_{0.5}Ca_{0.5}MnO_3$ ($A_{3.00}$) sample is in agreement with a perovskite-like orthorhombic structure[1] [a = 0.5407(2), b = 0.7629(2) and c = 0.5401(2) nm] with space group (SG) *Pnma*. A different situation is observed for the reduced sample, $La_{0.5}Ca_{0.5}MnO_{2.5}$ ($R_{2.50}$), which can be indexed on the basis of a brownmillerite unit cell[14] with parameters a = 0.5361(3), b = 1.6463(9) and c = 0.5340(3) nm (SG *Ibm*2) as a consequence of ordering of anionic vacancies. This structure can be described as an alternating sequence of octahedral and tetrahedral layers along the b direction of the perovskite subcell (Figure 1). The SAED and HREM study is in agreement with this model. Figure 2 shows a SAED pattern and its corresponding HREM image along [10$\bar{1}$] zone axis. An image calculation was performed taking into account the given unit cell and the atomic parameters characteristic of the brownmillerite structure.[13] A good agreement between experimental and calculated image (Figure 2, c) is observed. The charge balance in $La_{0.5}Ca_{0.5}MnO_{2.5}$ corresponds to a Mn average oxidation state of 2.50, which would fit to 50% of Mn^{3+} and 50% of Mn^{2+}. This is an unexpected situation since it would involve a smaller b parameter than the experimental one.[13] Considering the ionic radius[24] and the oxygen content, a more plausible situation would be 75% of Mn^{2+} and 25% of Mn^{4+}, although obviously an experimental measurement of the oxidation states is required.

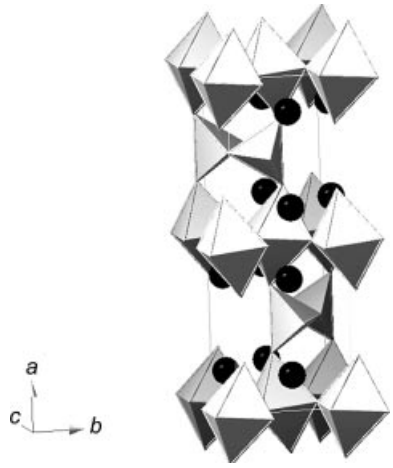

Figure 1. Brownmillerite structural model showing the alternating sequence of octahedral and tetrahedral layers along the b direction.

In order to determine the oxidation state of Mn in these materials, a detailed XANES study was performed. XANES spectra were treated quantitatively by using a factorial analysis taking into account the reference compounds spectra. This method was based on the modelling of the experimental spectra by means of a linear combination of reference spectra. The first step was to analyse well-defined patterns for the different oxidation states that Mn can adopt. In this sense, three different manganese compounds, MnO_2, $LaMnO_3$ and $MnCO_3$, exhibiting the three characteristic oxidation states Mn^{4+}, Mn^{3+} and Mn^{2+}, respec-

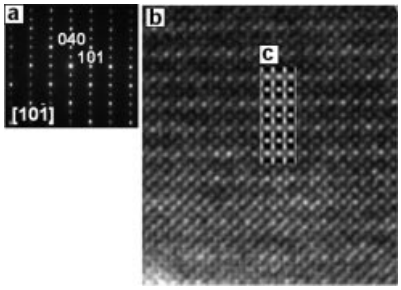

Figure 2. (a) SAED diffraction pattern along [10$\bar{1}$] zone axis; (b) HREM image; (c) calculated image taking into account the brownmillerite atomic positions.

tively, were used. Note that a perovskite-related compound $LaMnO_3$ was chosen as Mn^{3+} standard, while an oxide and a carbonate were selected for Mn^{4+} and Mn^{2+}, respectively. This was done because manganese perovskite-related phases only containing Mn^{4+} or Mn^{2+} have not been stabilized in the $La_{1-x}Ca_xMnO_3$ system. In fact, $CaMnO_3$ is always slightly deficient ($CaMnO_{3-\delta}$), leading to a small fraction of Mn^{3+}. In this sense, MnO_2 was used for Mn^{4+}. However, MnO was not used as the standard for Mn^{2+} because Mn_3O_4 impurities were detected by magnetic measurements, and thus $MnCO_3$ was considered more appropriate. In addition, we compared these data with already published standards of Mn^{4+}[25] and Mn^{2+}.[26]

The spectra in Figure 3 (a–c) show the Mn L-edge of the three different manganese compounds. For MnO_2 and $LaMnO_3$, the Mn L-edge spectra (Figure 3, parts a and b, respectively) present two main maxima, at 643 and 653 eV, which are accompanied by fine modulation. In fact, the first maximum of the MnO_2 spectrum shows a shoulder around 640 eV. Similar features are observed for the Mn L-edge spectrum of $LaMnO_3$. For Mn^{2+}, the main feature is a well-defined maximum at 641.2 eV accompanied by two small peaks at 640.5 and 642.7 eV. More pronounced differences are observed in the O K-edge spectra in the 528–538 eV range (Figure 4). Actually, Mn^{4+} shows two peaks: a more intense peak located at 529 eV and a second peak at 531.8 eV. For Mn^{3+}, the spectrum shows two broad maxima accompanied by fine modulation, whereas the Mn^{2+} shows only a peak located at 533.5 eV. Once the characteristic energies of Mn^{4+}, Mn^{3+} and Mn^{2+} have been established, the XANES spectra of the manganese materials can be more easily interpreted. Parts d and e in Figure 3 show the Mn L-edge XANES spectra of $A_{3.00}$ and $R_{2.50}$ samples, respectively. For $A_{3.00}$, two main peaks and a shoulder (around 641 eV) appear, as observed in MnO_2 and $LaMnO_3$, suggesting the presence of both Mn^{3+} and Mn^{4+}. $R_{2.50}$ exhibits similar features but the shoulder is transformed into a clear peak around 641 eV, which could be related to the presence of Mn^{2+}. In order to get more reliable information, the O K-edge spectra were studied (Figure 4, d and e). For $A_{3.00}$, the spectrum shows a profile characteristic of the coexistence of Mn^{3+} and Mn^{4+}, in agreement with the O K-edge of the reference materials. The spectrum corresponding to $R_{2.50}$ (Figure 4, e) shows a clear peak at around 533 eV which, in agreement with the O K-edge of the reference, is related to Mn^{2+}. Moreover, two more peaks appear at 529 and 536 eV indicating the presence of Mn^{4+} and Mn^{3+}, respectively. The data set of O K-edge and Mn L-edge of $A_{3.00}$ and $R_{2.50}$ XANES spectra were quantitatively treated, taking into account the reference compounds spectra, as depicted in Table 1. The ensemble of these results shows the coexistence of Mn^{2+}, Mn^{3+} and Mn^{4+} in $La_{0.5}Ca_{0.5}MnO_{2.5}$, obtained through the topotactic reduction process $A_{3.00} \rightarrow R_{2.50}$.

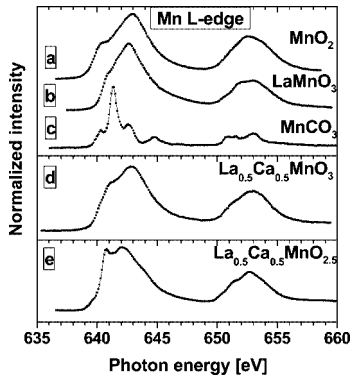

Figure 3. Mn L-edge XANES spectra of manganese reference compounds (a) MnO_2; (b) $LaMnO_3$; (c) $MnCO_3$ and samples (d) $La_{0.5}Ca_{0.5}MnO_3$; (e) $La_{0.5}Ca_{0.5}MnO_{2.5}$.

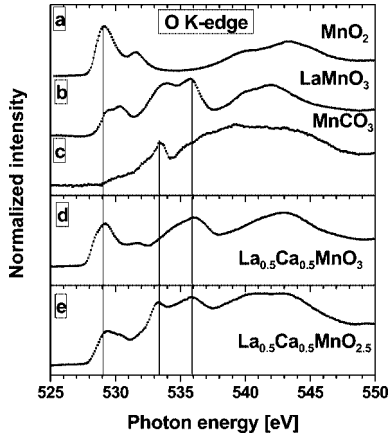

Figure 4. O K-edge XANES spectra of manganese reference compounds (a) MnO_2; (b) $LaMnO_3$; (c) $MnCO_3$ and samples (d) $La_{0.5}Ca_{0.5}MnO_3$; (e) $La_{0.5}Ca_{0.5}MnO_{2.5}$.

Table 1. Mn oxidation state of $A_{3.00}$ and $R_{2.50}$ samples as determined by XANES.

Sample	% Mn^{4+}	% Mn^{3+}	% Mn^{2+}
$A_{3.00}$	50.00	50.00	0
$R_{2.50}$	12.50	25.00	62.50

The oxidation process $R_{2.50} \rightarrow A_{3.00}$ is again a topotactic one involving the transformation of brownmillerite to perovskite.[27] At this point, in order to ascertain whether or not samples with the same composition comprise the same oxidation states, the oxidation mechanism was studied, since different pathways would involve different oxidation states and properties.

The influence of the anionic vacancies concentration in the crystalline structure and magnetotransport properties of samples obtained by reduction of the $La_{0.5}Ca_{0.5}MnO_3$ material has already been studied by several authors.[11–13] It has been shown that for a small concentration of anionic vacancies the CO state disappears whereas the ferromagnetic character is preserved. In particular, according to Trukhanov et al.,[12] the anionic vacancies originated in the reduction process are randomly distributed and the orthorhombic symmetry of the starting material remains up to δ = 0.25 ppm. However, when samples are obtained by oxidation of $R_{2.50}$, monophasic materials are only obtained, under the synthetic conditions described in ref.,[25] for $\delta <$ 0.15. For this reason, the comparative study of R_y and O_y materials was limited to the $0 \leq \delta \leq 0.12$ range.

All R_y and O_y materials show very similar X-ray diffraction patterns, which can be indexed on the basis of an orthorhombic symmetry and space group *Pnma*. All samples were characterized by SAED and HREM. Electron diffraction patterns did not show superstructure spots, suggesting that anionic vacancies in both R_y and O_y samples are randomly distributed in the $0 \leq \delta \leq 0.12$ range.

As in the starting materials, a detailed XANES study was performed. Figure 5 (a) shows the Mn L-edge XANES spectra of R_y samples. Taking into account the described reference patterns, spectra peaks suggest the presence of Mn^{3+} and Mn^{4+}. The spectra corresponding to the O K-edge (Figure 5, b) show maxima around 529 and 536 eV characteristic of Mn^{3+} and Mn^{4+}, respectively. Therefore, the reduction pathway $A_{3.00} \rightarrow R_{2.88}$ only involves the coexistence of both Mn^{4+} and Mn^{3+}. Figure 6 (a and b) show the Mn L-edge and O K-edge characteristics, respectively, of the oxidized samples. The presence of Mn^{3+} and Mn^{4+} is observed in Mn L-edge while an additional peak around 533 eV, suggesting Mn^{2+}, appears at the O K-edge. The quantification led to the results shown in Table 2, which confirm the presence of Mn^{3+} and Mn^{4+} in the R series while the three oxidation states Mn^{2+}, Mn^{3+} and Mn^{4+} coexist in the O series of samples. This table summarizes the fact that both topotactic reactions, $A_{3.00} \rightarrow R_{2.50}$ and $R_{2.50} \rightarrow A_{3.00}$, in the $0 \leq \delta \leq 0.12$ compositional range, occur through different pathways, that is, comprising different oxidation states. It is then clear that materials exhibiting the same composition but different electronic environment for Mn ions were stabilized. This should influence the properties, producing dramatic effects on the magnetic behaviour of these manganites.

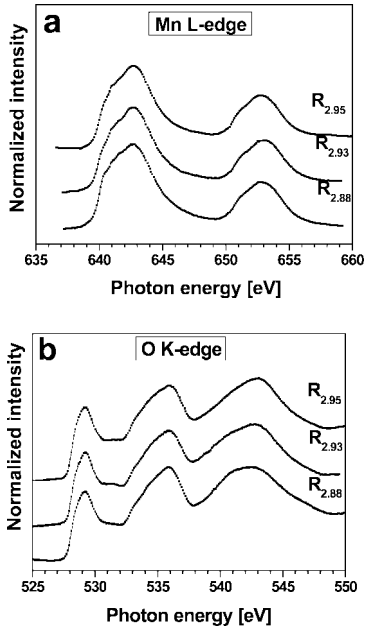

Figure 5. XANES spectra of R_y samples (a) Mn L-edge and (b) O K-edge.

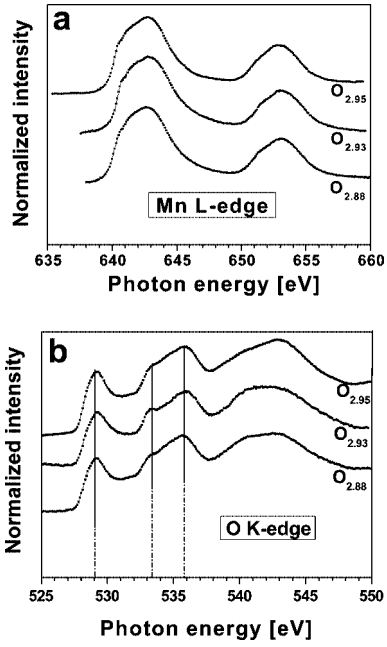

Figure 6. XANES spectra of O_y samples (a) Mn L-edge and (b) O K-edge.

Table 2. Mn oxidation state of R_y and O_y samples as determined by XANES.

Sample y	R_y % Mn (XANES)			O_y % Mn (XANES)		
	Mn^{4+}	Mn^{3+}	Mn^{2+}	Mn^{4+}	Mn^{3+}	Mn^{2+}
2.95	40.00	60.00	0.00	40.00	55.00	5.00
2.93	38.00	62.00	0.00	39.00	54.00	7.00
2.88	30.00	70.00	0.00	32.00	56.00	12.00

Figure 7 shows the temperature dependence of magnetization for $A_{3.00}$ and R_y samples. In agreement with previous results,[1,2,13] the fully oxidized $A_{3.00}$ sample shows a first transition from paramagnetic (PM) to almost FM at $T_C \approx 250$ K and a second transition at lower temperature to an AF state associated with CO of the charge carriers ($T_{CO} \approx 190$ K). At low temperature, a magnetization value of 0.25 μ_B/u.f. is still obtained since a 10% FM phase is observed despite the material being chemically homogeneous.[3,28] The reduction process of $A_{3.00}$ material involves the transformation of octahedra into square pyramids, inducing a rapid increase in the magnetization at low tem-

perature: 0.69 μ_B/u.f at 80 K for $R_{2.95}$. This fact is due to a partial breaking of the CO state which leads to a rapid increase in the FM fraction. A higher anionic vacancies concentration leads to a decrease in the magnetization for $R_{2.93}$ and $R_{2.88}$ samples. Similar behaviour was reported by Trukhanov et al.[12] where a maximum magnetization value was obtained for $y = 2.96$ and a minimum value for $y = 2.80$. This fact suggests that a high concentration of the anionic vacancies breaks the FM ordering due to a decrease in the Mn^{4+}/Mn^{3+} ratio and so allows the possibility of double exchange. In fact, when anionic vacancies content is increased to $\delta = 0.50$, the ferromagnetic interactions disappear as can be observed in the variation of the magnetization curve versus applied magnetic field (Figure 8).

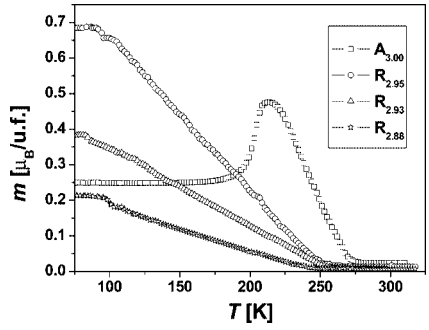

Figure 7. Magnetization vs. temperature corresponding to R_y samples.

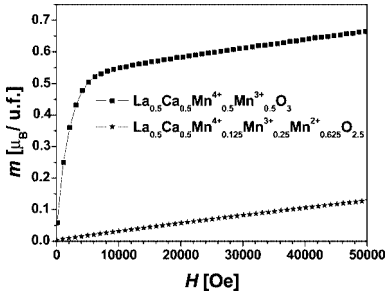

Figure 8. Magnetization vs. applied magnetic field at 5 K.

The magnetic behaviour of O_y materials (Figure 9) is different from that shown by R_y samples despite both composition and structure being identical. These oxidized samples show a first PM-FM transition: the magnetization value being higher for the $O_{2.95}$ sample. At 205 K, this sample shows again, although less markedly, the FM-AF transition associated with the CO observed in $A_{3.00}$. In fact, from 150 K, the magnetization corresponding to $O_{2.95}$ is lower than that observed for $O_{2.93}$, probably due to the presence of a higher number of AF regions in CO state, as a consequence of the lower Mn^{2+} content. The lowest oxygen-content sample, $O_{2.88}$, shows the highest 0.64 μ_B/u.f. magnetization value, which could be related to the absence of CO region in this composition. From the structural point of view,[29] the oxidation process leads to isolated rows of tetrahedrally coordinated Mn^{2+}, randomly distributed in an octahedrally coordinated Mn^{3+}–Mn^{4+} matrix, which accounts for the double exchange and, as a consequence, for FM behaviour. This situation is different from the one observed in the reduced sample of the same composition and can be explained taking into account structural considerations as well as the corresponding oxidation states. In this sense, for $O_{2.88}$ the FM ordering is locally broken due to the anionic vacancies concentrated around Mn^{2+}, whereas for $R_{2.88}$ it is associated with the vacancies around Mn^{3+}. In this last case, the number of Mn ions accompanied by a vacant is double than that in $O_{2.88}$ and, therefore, is also twice the number of positions where the double exchange is broken, leading to a lower magnetization value.

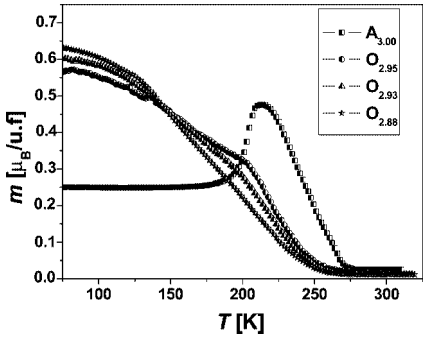

Figure 9. Magnetization vs. temperature corresponding to O_y samples.

Conclusions

The described results clearly show that the synthetic conditions play an important role in the stabilization of Mn oxidation state in perovskite-related materials. Numerous papers[11–13] have been devoted to studying the influence of an oxygen content change on the magnetic properties of these manganites. Up to now, it has been considered that the introduction of anionic vacancies only affects the Mn^{4+}/Mn^{3+} ratio. We have shown that, as a function of the synthetic pathway, Mn^{2+} can also be stabilized, leading to materials with Mn in three oxidation states.

Experimental Section

Two materials with the composition $La_{0.5}Ca_{0.5}MnO_3$ ($A_{3.00}$) and $La_{0.5}Ca_{0.5}MnO_{2.5}$ ($R_{2.50}$) were initially prepared. The starting material, $A_{3.00}$, was prepared by solid-state reaction of stoichiometric amounts of La_2O_3, $CaCO_3$ and MnO_2 at 1400 °C in air for 110 h. $La_{0.5}Ca_{0.5}MnO_{2.5}$ was obtained under controlled reduction of the $La_{0.5}Ca_{0.5}MnO_3$ sample. The reduction process was performed in a CAHN D-200 electrobalance, equipped with a furnace and a two-channel register, by heating the starting material at 630 °C under H_2 (200 mbar) and He (300 mbar) at 6 °C min^{-1}. Once a desired weight loss was attained, the sample was annealed at 630 °C, under He, for 24 h to facilitate a more homogeneous distribution of anionic vacancies. The oxygen content can be determined within $\pm 10^{-3}$ for a sample of total mass about 100 mg. Oxygen content

(as determined in this reduction process) and cationic composition of both materials (as determined by atomic absorption, plasma source emission spectroscopy and electron probe microanalysis) are in agreement with the nominal composition.

On the other hand, two series of samples $La_{0.5}Ca_{0.5}MnO_{3-\delta}$ were prepared by two different synthetic routes: (i) samples R_y, obtained by reduction of $La_{0.5}Ca_{0.5}MnO_3$ and (ii) samples O_y, after oxidation of $La_{0.5}Ca_{0.5}MnO_{2.5}$ until reaching, in both cases, the desired oxygen content y ($y = 3 - \delta$). Reduced $R_{2.95}$, $R_{2.93}$ and $R_{2.88}$ samples were obtained from $A_{3.00}$ under H_2 (200 mbar) and He (300 mbar) around 450 °C, whereas oxidized $O_{2.95}$, $O_{2.93}$ and $O_{2.88}$ materials were obtained from $R_{2.50}$ under O_2 (100 mbar) and He (400 mbar) around 170 °C. Both series were synthesized in an electrobalance allowing rigorous control of the oxygen content.

Powder X-ray diffraction (XRD) was performed by using a Philips X'Pert diffractometer with Cu-K_α radiation. Selected area electron diffraction (SAED) was performed by using a JEOL 2000FX electron microscope fitted with a double tilting goniometer stage (±45°), and high resolution electron microscopy (HREM) was carried out with a JEOL 3000FEG electron microscope fitted with an Oxford LINK EDS analyser. The sample was ultrasonically dispersed in 1-butanol and then transferred to holey carbon-coated copper grids. Magnetic properties were obtained using a LDJ vibrating sample and Quantum Design SQUID magnetometers in the temperature range 5 to 350 K under applied fields up to 5 T. Magnetic measurements versus temperature (5–350 K) were performed under field cool conditions in a 1000 Oe applied magnetic field. Magnetization measurements versus magnetic field (0–5 T) were carried out at 5 K.

Both Mn L-edge and O K-edge XANES measurements were performed using the PGM monochromator of the SU8 undulator-beamline at LURE. The spectra were collected in the total electron yield mode measuring the sample current. The energy resolution at the O K-edge and Mn L-edge X-ray absorption edge, around 530 and 643 eV was better than 0.5 and 0.6 eV, respectively. The surface sensibility of the XANES total yield technique was evaluated for these particular samples, recording the same absorption spectra by using the photoelectron effect. In this case, the detector was the photoelectron current recorded at the analyser. As the excited electrons should leave the solid to be collected at the vacuum, this recording mode is particularly sensible to the surface. A close comparison of XANES spectra recorded by both methods, evidences that surface effects can be ignored. The base pressure in the experimental chamber was in the low 10^{-10} mbar range. The samples were scraped in situ with a diamond file to remove surface contamination. Before every experiment, the samples were refreshed in order to avoid the formation of any stable carbonate. High level of sample cleanliness was guaranteed by synchrotron radiation core level photoemission continuous checking throughout the experiment. In particular, the evolution of the shape and intensity of the O K-edge and C K-edge core levels were monitored before and after the absorption measurements. As the valence band states near the Fermi level have shown to be very sensitive to external agents and spurious contamination, this kinetic energy range was monitored for all investigated samples.

Acknowledgments

Financial support through the Ministerio de Educación y Ciencia (MEC), Spain MAT2004-01248 is acknowledged.

[1] C. H. Chen, S.-W. Cheong, *Phys. Rev. Lett.* **1996**, *76*, 4042–4045.
[2] P. G. Radaelli, D. E. Cox, M. Marezio, S.-W. Cheong, *Phys. Rev. B* **1997**, *55*, 3015–3023.
[3] G. Xiao, E. J. McNiff Jr, G. Q. Gong, A. Gupta, C. L. Canedy, J. Z. Sun, *Phys. Rev. B* **1996**, *54*, 6073–6076.
[4] S. Mori, C. H. Chen, S.-W. Cheong, *Phys. Rev. Lett.* **1998**, *81*, 3972–3975.
[5] J. Herrero-Martín, J. García, G. Subías, J. Blasco, M. C. Sánchez, *Phys. Rev. B* **2004**, *70*, 024408.
[6] L. Brey, *Phys. Rev. Lett.* **2004**, *92*, 127202.
[7] M. Coey, *Nature* **2004**, *430*, 155–157.
[8] G. C. Milward, M. J. Calderon, P. B. Littlewood, *Nature* **2005**, *433*, 607–610.
[9] P. Schiffer, A. P. Ramirez, W. Bao, S.-W. Cheong, *Phys. Rev. Lett.* **1995**, *75*, 3348–3351.
[10] C.-W. Cheong, H. Y. Hwang, "Ferromagnetism vs. Charge/Orbital Ordering in Mixed-Valent Manganites" in *Advances in Condensed Matter Science*, vol. 2: *Colossal Magnetoresistance Oxides* (Ed.: Y. Tokura), Gordon & Breach Science Publishers, London, **2000**.
[11] W. Schuddinck, G. Van Tendeloo, C. Martin, M. Hervieu, B. Raveau, *J. Alloys Compd.* **2002**, *333*, 13–20.
[12] S. V. Trukhanov, N. V. Kasper, I. O. Troyanchuk, M. Tovar, H. Szymczak, K. Bärner, *J. Solid State Chem.* **2002**, *169*, 85–95.
[13] J. M. González-Calbet, E. Herrero, N. Rangavittal, J. M. Alonso, J. L. Martinez, M. Vallet-Regí, *J. Solid State Chem.* **1999**, *148*, 158–168.
[14] M. Von Harder, Hk. Müller-Buschbaum, *Z. Anorg. Allg. Chem.* **1980**, *464*, 169–175.
[15] A. Reller, J. M. Thomas, D. A. Jefferson, M. K. Uppal, *Proc. R. Soc. Lond. A* **1984**, *394*, 223–241.
[16] M. L. Ruiz-González, R. Cortés-Gil, J. M. Alonso, A. Hernando, M. Vallet-Regí, J. M. González-Calbet, *Chem. Mater.* **2006**, *18*, 5756–5763.
[17] J. A. M. van Roosmalen, E. H. P. Cordfunke, *J. Solid State Chem.* **1994**, *110*, 109–112.
[18] J.-H. Choy, S.-T. Hong, N.-G. Park, S.-H. Byeon, G. Demazeau, *Bull. Korean. Chem. Soc.* **1995**, *16*, 105–110.
[19] A. C. Scheinost, H. S. Darrell, G. Schulze, U. Gasser, D. L. Sparks, *Am. Miner* **2001**, *86*, 139–146.
[20] F. Bridges, C. H. Booth, G. H. Kwei, J. J. Neumeier, G. A. Sawatzky, *Phys. Rev. B* **2000**, *61*, R9237–R9240.
[21] J. C. Fuggle, J. E. Inglesfield, *Unoccupied Electronic States*, Springer, Berlin, **1982**.
[22] M. Abbate, F. M. F. de Groot, J. C. Fuggle, A. Fujimori, Y. Tokura, Y. Fujushima, O. Strebel, M. Domke, G. Kaindl, J. van Elp, B. T. Thole, G. A. Sawatzky, M. Sacchi, N. Tsuda, *Phys. Rev. B* **1991**, *44*, 5419–5422.
[23] M. Abbate, F. M. F. de Groot, J. C. Fuggle, A. Fujimori, O. Strebel, F. Lopéz, M. Domke, G. Kaindl, G. A. Sawatzky, M. Takano, Y. Takeda, H. Eisaki, S. Uchida, *Phys. Rev. B* **1992**, *46*, 4511–4519.
[24] R. D. Shannon, *Acta Crystallogr., Sect. A* **1976**, *32*, 751–767.
[25] M. Abbate, D. Z. N. Cruz, G. Zampieri, J. Briatico, M. T. Causa, M. Tovar, A. Caneiro, B. Alascio, E. Morikawa, *Solid State Commun.* **1997**, *103*, 9–13.
[26] B. Gilbert, B. H. Frazer, A. Belz, P. G. Conrad, K. H. Nealson, D. Haskel, J. C. Lang, G. Srajer, G. De Stasio, *J. Phys. Chem. A* **2003**, *107*, 2839–2847.
[27] M. Vallet-Regí, E. Herrero, J. Alonso, A. Hernando, J. M. González-Calbet, *Solid State Ionics* **2001**, *141–142*, 427–432.
[28] R. S. Freitas, L. Ghivelder, P. Levy, F. Parisi, *Phys. Rev. B* **2002**, *65*, 104403.
[29] S. Komornicki, J. C. Grenier, M. Pouchard, P. Hagenmuller, *Nuovo J. Chim.* **1981**, *5*, 161–168.

Received: January 26, 2007
Published Online: June 1, 2007

